9th International Conference on Fibre-Reinforced Polymer (FRP) Composites in Civil Engineering (CICE 2018), PARIS 17-19 JULY 2018

SPLICE CONNECTION FOR TUBULAR FRP COLUMN MEMBERS

C. Qiu [1], Y. Bai [2]
[1] *Department of Civil Engineering, Monash University, Australia*
[2] *Department of Civil Engineering, Monash University, Australia, Email: yu.bai@monash.edu*

ABSTRACT

Pultruded fibre reinforced polymer (FRP) members are increasingly favoured in civil engineering as they are lightweight and corrosion-resistant. However, their application is limited by the challenge to connect them, especially tubular members, i.e. with closed sections. A splice connection is developed in this paper for tubular FRP members and its mechanical performance under axial and flexural loadings is investigated. The developed splice connection entails two tubular steel-FRP bonded sleeve joints (BSJs) and a steel bolted flange joint (BFJ) in between. Experimental tests were conducted on the splice connections of varied bond lengths and bolt configurations; results are reported and discussed regarding failure mode, load-displacement behaviour and strain response. The experimental investigation revealed that an effective bond length exists for the BSJs under axial loading, and that an eight-bolt configuration for the BFJ is more effective compared to a four-bolt one in terms of tensile and rotational stiffness and strength. Besides, it is concluded that the splice connection can be designed to fail in a ductile manner under both axial and flexural loadings.

KEYWORDS

Fibre reinforced polymer (FRP), tubular member, splice connection, experimental study, axial loading, flexural loading.

INTRODUCTION

Fibre reinforced polymer (FRP) structural members manufactured from the pultrusion process are credited with high strength-to-weight ratio, excellent corrosion resistance, and availability in various section shapes (Bank 2006). However, connecting FRP structural members into assembly is challenging, especially for tubular members, due to the closed section shape and the brittle and anisotropic nature of the materials. Early efforts to connect pultruded FRP I-sections into frame structure adopted bolted flange and web seated angles made of FRP (Bank et al. 1994). Steel seated angles were later proposed to prevent local failure in the connectors (Mottram and Zheng 1996). Utilising the steel flange seated angles and also bolted-through web-gusset plates, FRP tubular members were joined into beam-column assembly (Smith et al. 1999). Tubular FRP-steel bolted sleeve joints were proposed for assembly of space lattice structures and studied under axial loadings (Luo et al. 2015). It was found that bolt fastening caused stress concentration and exposed the weak in-plane shear strength of the FRP composites. To achieve more uniform stress transfer through adhesive bonding, bonded sleeve connections for joining circular FRP truss members into space frames using nodal joints were proposed and examined by Yang et al. (2016). In an experimental investigation by Wu et al. (2016), the bonded sleeve connection was applied in a tubular FRP beam-to-steel column assembly, exhibiting significant improvement in both rotational strength and stiffness over steel angle connections and bolted sleeve connections.

Despite the aforementioned works, research into developing a splice connection for FRP tubular members in column applications is still limited. Inspired by the previous success of the FRP-steel bonded sleeve connection concept, this paper proposes a splice connection for tubular glass FRP (GFRP) members and investigates experimentally its performance under axial and flexural loadings. Figure 1 illustrates the proposed splice connection and provides reference dimensions for this study. The proposed connection consists of a bonded sleeve joint (BSJ) coupling steel and GFRP tubes adhesively, and a bolted flange joint (BFJ) connecting two steel tubes with flange plates by bolts. When used as a column splice, the connection would be subjected to axial or flexural loadings or a combination of both. In this paper, the axial behaviour of the splice connection is investigated by testing the BSJ and the BFJ individually; while the flexural behaviour is studied by subjecting the connection to pure moment loading.

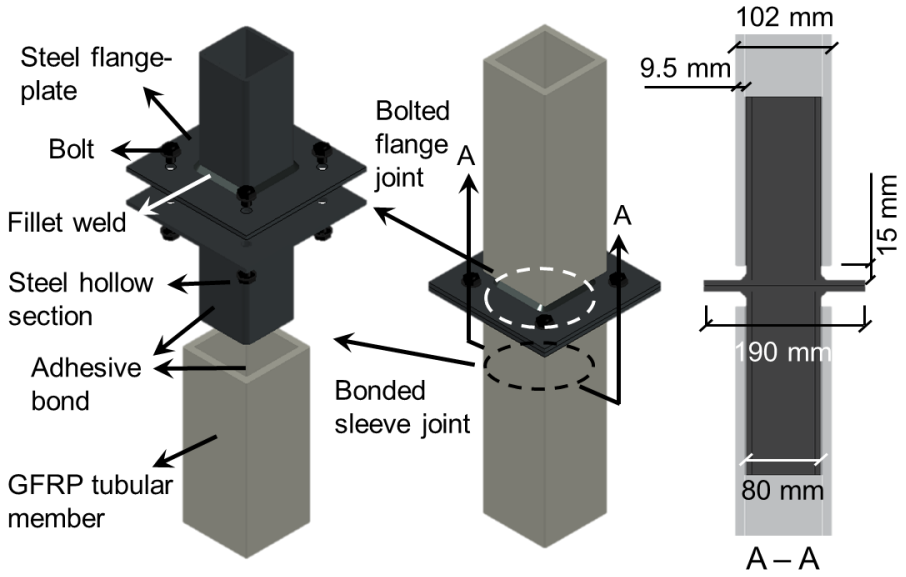

Figure 1: Proposed splice connection for tubular FRP members

EXPERIMENT PROGRAM

Specimens and material properties

All the specimens for axial and flexural loadings are indexed as in Table 1, where the first letter refers to the loading type ('A' for axial and 'B' for bending). Only compression tests were conducted on the A-BSJ (bonded sleeve joint for axial loading) specimens, as theoretical and numerical studies revealed that, considering cohesive failure as the failure mode of interest, tensile and compressive loadings would induce identical adhesive shear stress distribution along the bond length and thus identical joint behaviour (Qiu et al. 2017). For the A-BFJs, compressive failure would be preceded by member failure of the connected steel hollow section member, therefore only the tensile behaviour of the A-BFJs (bolted flange joint for axial loading) was investigated.

Each of the A-BSJ specimens, with geometries illustrated in Figure 2 (a), was assembled by coupling a pultruded GFRP square tube (102 × 102 × 9.5 mm) and a steel square hollow section (SHS, 80 × 80 × 6 mm) with Sikadur-30, a two-component epoxy-based adhesive; four different bond lengths were covered as listed in Table 1. Although an adhesive layer around 0.5 mm in thickness is recommended for strong and reliable binding (Arenas et al. 2010), a 1.5 mm-layer thickness is selected in this study to provide tolerance for geometric imperfection of the cross sections and practical fabrication. Shown in Figure 2 (b), the A-BFJ specimens were fabricated by bolting (high strength M12 bolts) two 6 mm-thick steel flange-plates each of which was welded to a steel SHS (same as those in A-BSJs); a gusset plate was also slot-welded into the steel SHS for application of tensile loading. Figure 2 (c) presents the two bolt configurations adopted in the A-BFJ and the bending specimens. Two specimens, namely B-170-4 and B-120-8, were prepared for flexural loading, with their configurations and geometries described in Table 1 and Figure 2 (d). In the bending specimens, the steel flange-plates and the SHSs are the same as those used in the A-BSJs and A-BFJs, so is the cross-section geometries of the GFRP tubes; while the GFRPs were sourced from another supplier and a less viscous adhesive (Sikadur-330) was adopted for easier fabrication of the specimens. Material properties of the components used in the aforementioned specimens were summarised in Table 2.

Table 1: Specimens for axial and flexural loading

Specimen index*	Loading	Bond length (mm)	NO. of bolts	GFRP	Adhesive
A-BSJ-50-1, 2	Axial compression	50	-	White	Sikadur-30
A-BSJ-100-1, 2		100	-		
A-BSJ-140-1, 2		140	-		
A-BSJ-180-1, 2		180	-		
A-BFJ-4-1, 2	Axial tension	-	4	-	-
A-BFJ-8-1, 2		-	8	-	-
B-170-4	Four-point bending	170	4	Grey	Sikadur-330
B-120-8		120	8		

* Beside the bending specimens B-170-4 and B-120-8, two repeating specimens were prepared, indicated by the last number in the specimen index.

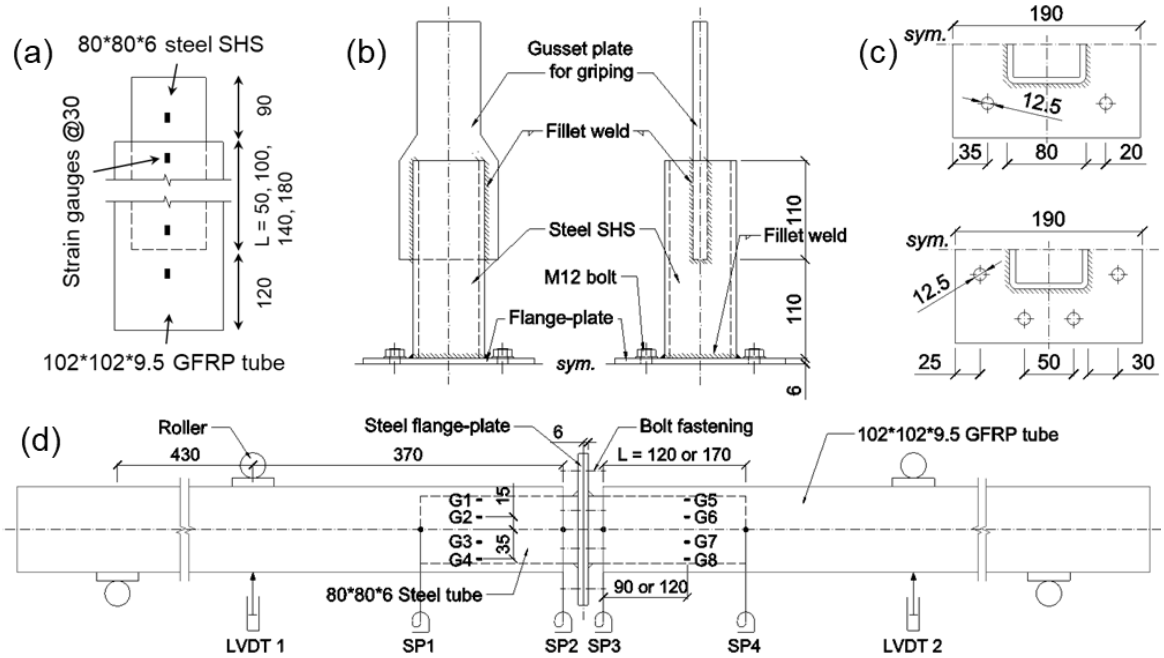

Figure 2: Geometries (all units in mm) and instrumentations (a) A-BSJ specimens; (b) A-BFJ specimens; (c) steel flange-plates for A-BFJ and bending specimens; (d) bending specimens B-170-4 or B-120-8

Table 2: Material properties

Material	Modulus [1] (GPa)	Strength [2] (MPa)	Poisson's ratio
Steel flange	200.6	313.6	0.277
Steel SHS	209.5	420.1	0.277
GFRP tube-white	30.2/5.5/3.5	306.5/-/26.7	-
GFRP tube-grey	25.2/6.2/3.0	330.6/88.5/31.2	0.280
Sikadur-30	11.2	22.4	0.310
Sikadur-330	4.2	32.8	0.280

[1]: Young's modulus for steels and adhesives; longitudinal tensile/transverse tensile/shear modulus for GFRPs
[2]: Yiled strength for steels; longitudinal tensile/transverse tensile/shear strength for GFRPs; tensile strength for adhesives

Setup and instrumentation

Compressive loading on the A-BSJ specimens was implemented by a 500 kN Amsler machine at 0.4 mm/min loading rate (Figure 3 (a)). Axial shortening of the specimens was measured by two linear variable differential transducers (LVDT). As shown in Figure 2 (a), strain gauges were installed on the surface of the steel SHS and the GFRPs at 30 mm intervals. Tensile loading on the A-BFJ specimens was applied by a 500 kN Baldwin machine at 0.5 mm/min loading rate (Figure 3 (b)). A laser extensometer was used to gauge axial elongation of the

specimens. As depicted in Figure 2 (d) and Figure 3 (c), the bending specimens were loaded in a four-point bending setup to subject the splice connection to pure moment loading. Via a 200 kN Amsler machine, the bending action was applied by locking the two upper rollers while lifting the two lower ones at 1.5 mm/min. Strain gauges G1 to G8 were installed on the side surface of the GFRP-steel combined section as described in Figure 2 (d). Two LVDTs and four string pots (SPs) were deployed to measure deflection of the specimens.

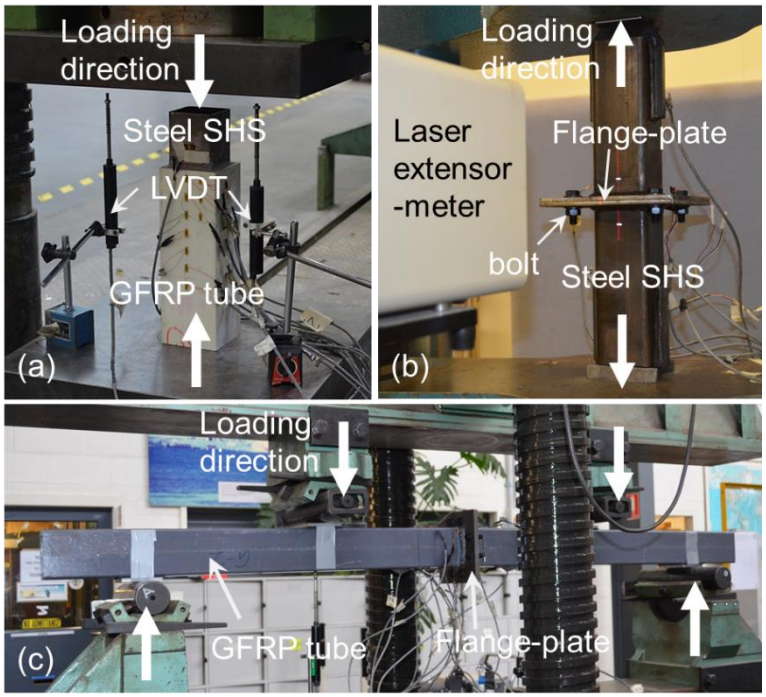

Figure 3: Experimental setup (a) A-BSJ specimens under compression; (b)A-BFJ specimens under tension; (c) bending specimens under four-point bending

RESULTS AND DISCUSSIONS

Load-deflection behaviours and failure modes

For all the A-BSJ specimens, experiments revealed a brittle cohesive failure within the adhesive layer. Upon failure, cracking in the adhesive layer occurred as shown in Figure 4 (a). Figure 4 (b), representative of all the A-BSJs, shows the separated adherends and the crack surface where bond failure occurred; the attachment of adhesive to both the steel and GFRP indicates cohesive failure located within the adhesive layer. Figure 4 (c) shows the typical load-displacement curves, characterised by linear increase before brittle failure. Post-failure residual strength, due to the friction between the fracture surfaces, was recorded between 10 to 45 kN among the specimens. Joint capacities of the A-BSJs (P_u) are plotted versus the bond lengths (L) in Figure 4 (d). The joint capacity P_u increases almost linearly with L up to $L = 100\ mm$; while from $L = 100\ mm$ to $180mm$ the improvement of P_u slows down dramatically, by a mere 18 % (from an average of 284.5 kN to 336.0 kN), which indicates the existence of an effective bond length around 100 mm.

All the A-BFJ specimens failed by steel yielding of the flange-plates. As shown in Figure 5 (a), elongation of A-BFJ-4 (i.e. A-BFJ with four bolts) resulted in opening gaps between the two flange-plates in the region away from the bolts; while in A-BFJ-8, the flange-plates were bent outwards in the regions between the bolts and the SHS (Figure 5 (b)). Figure 5 (c) presents the tensile load-displacement curves of the A-BFJs. After steel yielding, the curves kept increasing gradually at near constant slopes until the loading process was ceased at 9 mm-elongation for the A-BFJ-4s or at 8 mm for the A-BFJ-8s. Defined as the intersection point of the elastic and hardening tangent line, an average yield load is obtained as 104.2 kN for A-BFJ-4 and 183.8 kN for A-BFJ-8. The average initial stiffness of A-BFJ-4 and A-BFJ-8 is 104 kN/mm and 346 kN/mm respectfully. It can be found that the eight-bolt configuration results in an increase of 77 % in yield load and 233 % in initial stiffness when compared to the four-bolt configuration.

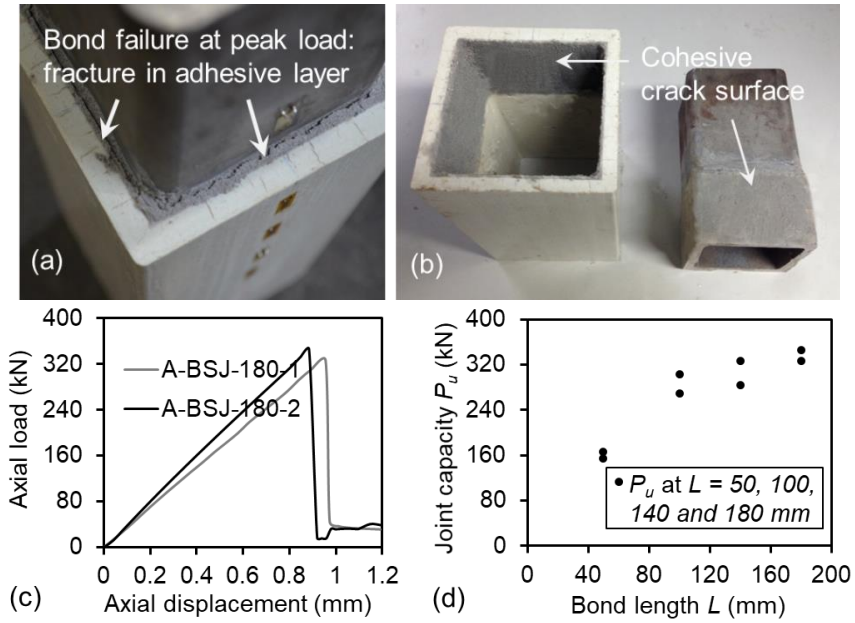

Figure 4: The A-BSJ specimens (a) Adhesive failure at peak load; (b) Bond failure surface; (c) Typical compression-displacement curves of A-BSJs; (d) Joint capacity versus bond length

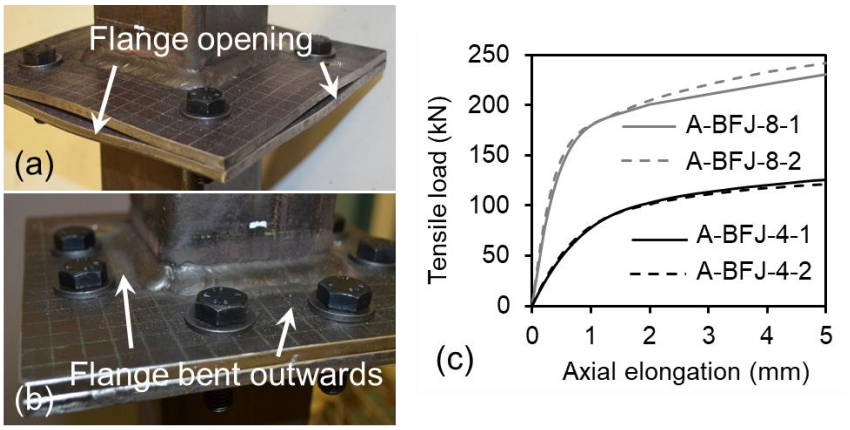

Figure 5: Deformed shape of (a) A-BFJ-4s, (b) A-BFJ-8s and (c) Tension-displacement curves of A-BFJs

The behaviour of the A-BSJ and A-BFJ specimens reported above illuminates the behaviour of the proposed splice connection (integrating the BSJ and the BFJ) under axial loadings. Under compressive loading, the behaviour of the splice connection is governed by the BSJ component: the load-displacement curve would be linear up to brittle failure in the BSJ, and an effective bond length would exist for the joint capacity as found with the A-BSJ specimens. Under tensile loading, the load-displacement behaviour of the splice connection would be linear before brittle bond failure in the BSJ, if the joint capacity of the BSJ is attained before yielding of the BFJ component. It is recommended that a sufficient bond length is designed such that the capacity of the BSJ is above the yield load of the BFJ to achieve a ductile failure. For example, in the case of a suggested specimen A-180-8 (integrating A-BSJ-180 and A-BFJ-8) under tensile loading, substantial energy would be dissipated through yielding of the steel flange-plate before adhesive failure in the BSJ. It should be noted that the bond failure in the BSJ may be preceded by failure in the GFRP, as buckling under compression or tensile failure, depending on the geometries and material properties of the GFRP and also the adhesive. In such cases, under compressive loading, connection failure would be shifted to member failure of the GFRP; under tensile loading, ductility of the BFJ should be utilized before brittle tensile failure of the GFRP.

Figure 6 presents the moment-rotation curves of the bending specimens B-170-4 and B-120-8, where the rotation angle α between the connected GFRP members is illustrated in Figure 7 (a) and calculated by Equation (1) shown below. The moment-rotation curve of B-170-4 starts to show nonlinearity at around 3.9 kNm, caused by yielding of the steel flange-plates. Loading of the specimen was continued until the displacement limit of the loading machine, where the bending moment barely increased (around 8.4 kNm as shown in Figure 6). Figure 7 (a) shows

the final overall deformation of B-170-4, no failure in the GFRP and the bonded region was observed. The final deformed shape of the flange-plates is indicated in Figure 7 (b), marked by the opening gaps at the sides and the bottom. For B-120-8, yielding of the steel flange-plates starts at around 7.8 kNm; the bending moment continues to increase at reduced rotational stiffness until a peak bending moment of 13.9 kNm where moment resistance of the specimen drops suddenly (Figure 6). Figure 7 (c) shows the final flange deformation of B-120-8; although not readily visible, the steel flanges were bent outwards between the steel SHS and the bolts at the tensile region. The final failure of B-120-8 was caused by cracking of the upper web-flange junctions of one of the GFRP tubes as indicated in Figure 7 (d); at the same time the GFRP was separated from the steel SHS at the bottom and sides due to cracking in the adhesive. From B-170-4 to B-120-8, the initial rotational stiffness does not see a notable increase (from 233 kNm/rad to 345 kNm/rad), while the yield moment (intersection point of the elastic and hardening tangent line) experiences a remarkable improvement by 86 %, from 5.6 kNm to 10.4 kNm.

$$\alpha = \frac{d_{SP1} - d_{LVDT1}}{L_{1,1}} + \frac{d_{SP4} - d_{LVDT2}}{L_{4,2}} \quad (1)$$

where d is the displacement measured by a LVDT or SP, $L_{x,y}$ is the horizontal distance between SP x and LVDT y (positions of LVDTs and SPs indicated in Figure 2 (d))

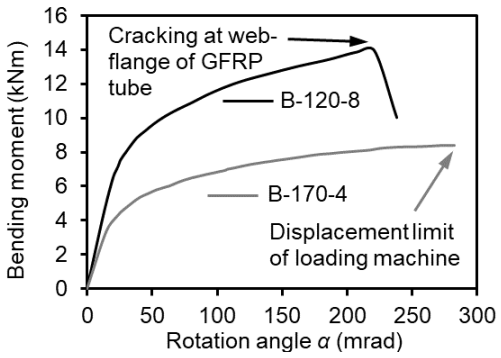

Figure 6: Moment-rotation curves of the bending specimens

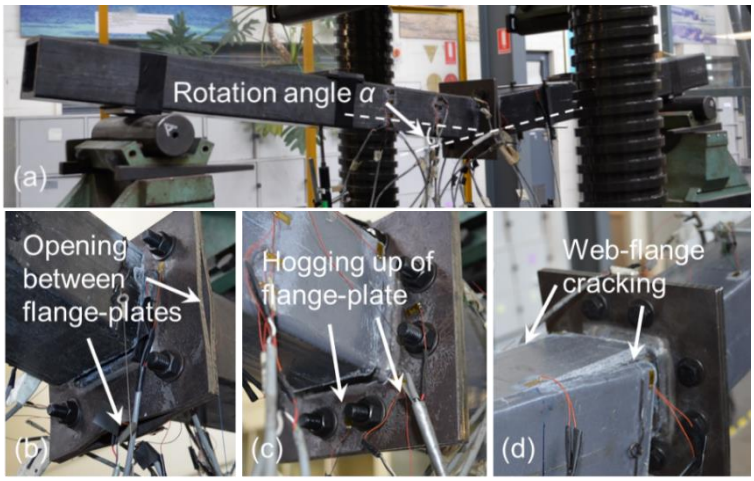

Figure 7: (a) Overall deformation B-170-4; (b) Final flange deformation of B-170-4; (c) Final flange deformation of B-120-8; (d) Web-flange cracking in the GFRP of B-120-8

Strain response

For the A-BSJ specimens, output from the strain gauges on the steel SHS and the GFRP tube indicated both the adherends within elastic range. From the specimen A-BSJ-180-2, axial strains on the outer surface of the GFRP, at four different load levels, are plotted along the centre bond line in Figure 8. It is found that the axial strain distribution at mid-portion of the bond length features a flatter gradient, revealing lower level of adhesive shear stress in this region than at the ends of the bond length. In general, the axial strain distribution near the GFRP end of the bond length ($x = 180$ *mm*) exhibits a steeper gradient than near the steel end ($x = 0$ *mm*). This is consistent with theory that greater shear slip between the adherends would be incurred near the more flexible adherend (GFRP in this case). Also noteworthy is that at 100% P_u, the strain distribution flattens near the GFRP end,

indicating a drop of the adhesive shear stress. This can be caused by softening of the Sikadur-30 adhesive, which was discovered, by a single lap pull-off test configuration, with an elastic-softening bond-slip behaviour (Yu et al. 2012).

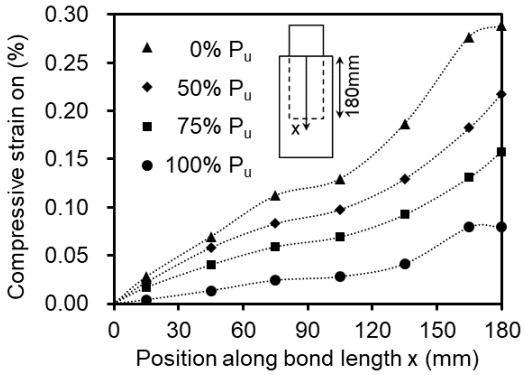

Figure 8: Axial strains on the GFRP along centre bond line (A-BSJ-180-2) at different load levels

For the bending specimens, the axial strain distribution on the side surface of the GFRP-steel composite section is plotted along the section depth in Figure 9. Corresponding to the specimen B-170-4 which failed due to excessive yielding of the steel flange-plates, Figure 9 (b) shows linear distribution of the axial strain along the section depth, revealing that composite action between the GFRP tube and the steel SHS was maintained from start to the ultimate bending moment (M_u). From the same strain gauges, the linear load-strain response presented in Figure 9 (b) indicates the BSJ components of the connection remained intact during the loading process.

Figure 9 (c) shows the axial strain distribution along section depth of B-120-8 which failed ultimately at the web-flange junction of the GFRP (Figure 7 (d)). Strain gauges G5 to G8 on the failed GFRP tube (instead of G1 to G4 on the intact GFRP tube) were selected to output the strain distribution. It is observed from Figure 9 (c) that the strain distribution is almost linear up to 75% M_u, but deviates from linearity at 100% M_u. This strain data is plotted as load-strain curves shown in Figure 9 (d). It is revealed that except for the G7 curve which maintains linear, the other load-strain curves develop in decreasing slope after around a bending moment of 8.5 kNm. This implies an incomplete stress transfer between the steel SHS and the GFRP, possibly caused by softening or cracking of the adhesive.

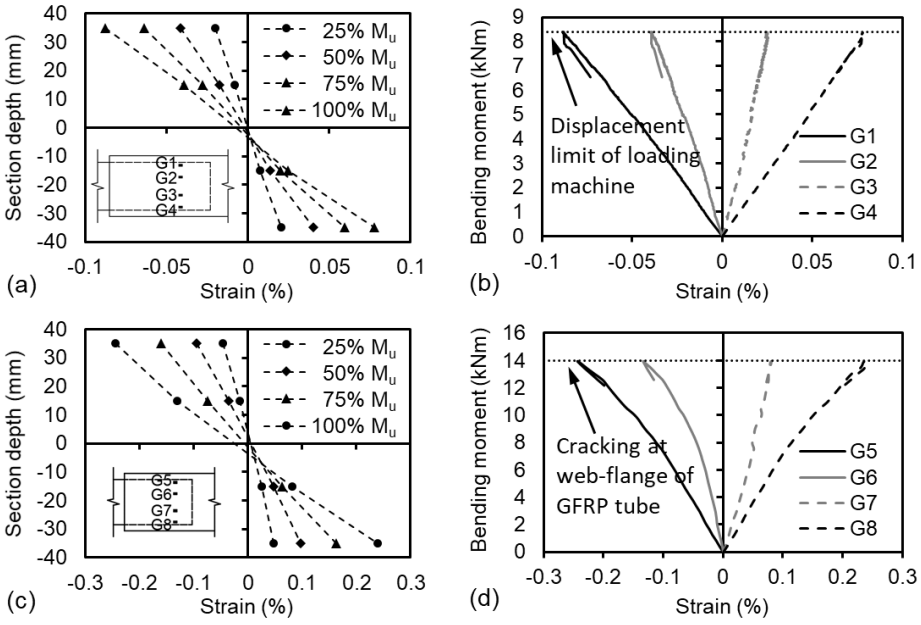

Figure 9: Strain response on the side surface of the steel-GFRP composite section (a) Axial strain distribution along section depth B-170-4; (b) Load-strain response B-170-4; (c) Axial strain distribution along section depth B-120-8; (d) Load-strain response B-120-8

CONCLUSIONS

In this paper a splice connection is introduced for joining FRP tubular column members. It is comprised of two tubular FRP-steel bonded sleeve joints (BSJ) and a steel SHS bolted flange joint (BFJ) in between. Experiments were conducted to investigate the mechanical performance of the connections under axial and flexural loadings. Based on the experimental results from specimens of varied bond lengths and two bolt configurations, the following conclusions can be drawn:

- Under axial loading the BSJs failed brittlely in the adhesive layer, and an effective bond length was found around 100 mm for the section geometries and the adhesive in this study. Strain distribution on the GFRP surface indicated softening of the adhesive near the GFRP end as the load increased. Failure of the BFJs under tensile loading was ductile through yielding of the steel flange-plates. The eight-bolt configuration (A-BFJ-4), compared to the four-bolt one (A-BFJ-4), improved the initial stiffness by 225% and the yield load by 82%. Integrating the BSJ and the BFJ, the splice connection can be designed with the 180 mm bond length and the eight-bolt configuration in this study, such that under tensile loading ductile failure would occur in the BFJ component before brittle failure in the BSJ.

- Under flexural loading the splice connection specimens experienced substantial yielding in the steel flange-plates. The B-170-4 specimen (with 170 mm bond length and the four-bolt configuration) remained intact in the BSJ component, while B-120-8 failed ultimately in the web-flange junction of the GFRP tube. With yielding of both the specimens governed by the BFJ component, the eight-bolt configuration was found to enhance the yield moment by 86 %, compared to the four-bolt one. Strain results indicated that full composite action in the BSJ was maintained in B-170-4, while softening or cracking of the adhesive might have occurred in B-120-8.

ACKNOWLEDGMENTS

The authors acknowledge the support from the Australian Research Council through the Discovery scheme (DP180102208). Thanks are also given to the staffs in the Civil Engineering Laboratory of Monash University for their technical supports.

REFERENCES

Arenas, J. M., Narbon, J. J., and Alía, C. (2010). "Optimum adhesive thickness in structural adhesives joints using statistical techniques based on Weibull distribution." *International Journal of Adhesion and Adhesives*, 30(3), 160-165.

Bank, L. C. (2006). *Composites for construction: structural design with FRP materials*, John Wiley & Sons.

Bank, L. C., Mosallam, A. S., and McCoy, G. T. (1994). "Design and performance of connections for pultruded frame structures." *Journal of reinforced plastics and composites*, 13(3), 199-212.

Luo, F. J., Bai, Y., Yang, X., and Lu, Y. (2015). "Bolted Sleeve Joints for Connecting Pultruded FRP Tubular Components." *Journal of Composites for Construction*, 04015024.

Mottram, J., and Zheng, Y. (1996). "State-of-the-art review on the design of beam-to-column connections for pultruded frames." *Composite structures*, 35(4), 387-401.

Qiu, C., Feng, P., Yang, Y., Zhu, L., and Bai, Y. (2017). "Joint capacity of bonded sleeve connections for tubular fibre reinforced polymer members." *Composite Structures*, 163, 267-279.

Smith, S., Parsons, I., and Hjelmstad, K. (1999). "Experimental comparisons of connections for GFRP pultruded frames." *Journal of Composites for Construction*, 3(1), 20-26.

Wu, C., Zhang, Z., and Bai, Y. (2016). "Connections of tubular GFRP wall studs to steel beams for building construction." *Composites Part B: Engineering*, 95, 64-75.

Yang, X., Bai, Y., Luo, F. J., Zhao, X.-L., and He, X.-h. (2016). "Fiber-Reinforced Polymer Composite Members with Adhesive Bonded Sleeve Joints for Space Frame Structures." *Journal of Materials in Civil Engineering*, 04016208.

Yu, T., Fernando, D., Teng, J., and Zhao, X. (2012). "Experimental study on CFRP-to-steel bonded interfaces." *Composites Part B: Engineering*, 43(5), 2279-2289.